Chemical Characterization of Submicron Aerosol and Particle Growth Events at a National Background Site (3295 m a.s.l.) on the Tibetan Plateau

W. Du[1,2], Y. L. Sun[1,*], Y. S. Xu[3], Q. Jiang[1], Q. Q. Wang[1], W. Yang[3], F. Wang[3], Z. P. Bai[3], X. D. Zhao[4], and Y. C. Yang[2]

[1]*State Key Laboratory of Atmospheric Boundary Layer Physics and Atmospheric Chemistry, Institute of Atmospheric Physics, Chinese Academy of Sciences, Beijing 100029, China*

[2]*Department of Resources and Environment, Air Environmental Modeling and Pollution Controlling Key Laboratory of Sichuan Higher Education Institutes, Chengdu University of Information Technology, Chengdu 610225, China*

[3]*Chinese Research Academy of Environmental Sciences, Beijing 100012, China*

[4]*National Station for Background Atmospheric Monitoring, Menyuan, Qinghai 810000, China*

*Correspondence to: Y. L. Sun (sunyele@mail.iap.ac.cn)

Abstract

Atmospheric aerosols exert highly uncertain impacts on radiative forcing and also have detrimental effects on human health. While aerosol particles are widely characterized in megacities in China, aerosol composition, sources and particle growth in rural areas in the Tibetan Plateau remain less understood. Here we present the results from an autumn study that was conducted from 5 September to 15 October 2013 at a national background monitoring station (3295 m a.s.l.) in the Tibetan Plateau. The submicron aerosol composition and particle number size distributions were measured in situ with an Aerodyne Aerosol Chemical Speciation Monitor (ACSM) and a Scanning Mobility Particle Sizer (SMPS). The average mass concentration of submicron aerosol (PM_1) is 11.4 μg m^{-3} (range: 1.0 - 78.4 μg m^{-3}) for the entire study, which is much lower than those observed at urban and rural sites in eastern China. Organics dominated PM_1 on average accounting for 43%, followed by sulfate (28%) and ammonium (11%). Positive matrix factorization analysis of ACSM organic aerosol (OA) mass spectra identified an oxygenated OA (OOA) and a biomass burning OA (BBOA). The OOA dominated OA composition accounting for 85% on average, 17% of which was inferred from aged BBOA. The BBOA contributed a considerable fraction of OA (15%) due to the burning of cow dung and straws in September. New particle formation and growth events were frequently observed (80% of time) throughout the study. The average particle growth rate is 2.0 nm hr^{-1} (range: 0.8 – 3.2 nm hr^{-1}). By linking the evolution of particle number size distribution to aerosol composition, we found an elevated contribution of organics during particle growth periods and also a positive relationship between the growth rate and the fraction of OOA in OA, which potentially indicates an important role of organics in particle growth in the Tibetan Plateau.

Keywords

Tibetan Plateau; ACSM; Submicron Aerosol; OOA; BBOA; Particle Growth

1 Introduction

High concentration of atmosphere aerosol associated with the rapid economic growth, urbanization and industrialization has become a major environmental concern in China. Aerosol particles especially fine particles ($PM_{2.5}$) have large impacts on human health, natural ecosystem, weather and climate, radiative balance and the self-purification capacity of troposphere (Jacobson, 2001; Tie and Cao, 2009). As a result, a large number of studies have been conducted to investigate the sources, chemical and physical properties, and evolution processes of aerosol particles at urban and rural sites in China during the last decade (Cao et al., 2007; Wu et al., 2007; He et al., 2011; Gong et al., 2012; Huang et al., 2012; Huang et al., 2013; Sun et al., 2013). The results showed that fine particles are mainly composed of organics, sulfate, nitrate, ammonium, mineral dust, and black carbon. The sources of organic aerosol (OA) were also characterized and various OA factors from distinct sources were identified including primary OA (POA), e.g., hydrocarbon-like OA (HOA), cooking OA (COA), biomass burning OA (BBOA) and coal combustion OA (CCOA), and secondary OA (SOA), e.g., semi-volatile oxygenated OA (SV-OOA) and low volatility OOA (LV-OOA) (Huang et al., 2010; Sun et al., 2010; He et al., 2011; Huang et al., 2011; Xu et al., 2014a). While previous studies significantly improve our understanding on the sources and chemical properties of aerosol particles, they were mainly conducted in developed areas in China, including Beijing-Tianjin-Hebei, Pearl River Delta and Yangtze River Delta.

The Tibetan Plateau (~ 2,000,000 square kilometers) is the highest plateau in the world with an average altitude of over 4000 meters above sea level. The Tibetan Plateau is an ideal location for charactering rural and regional background aerosol due to minor influences of anthropogenic activities. However, chemical characterization of aerosol particles in the Tibetan Plateau is rather limited, and therefore their sources, properties, and evolution processes are poorly known. Cong et al. (2015) reported the seasonal variations of various aerosol components including carbonaceous species and water-soluble ionic species on the south edge of the Tibetan Plateau. Sulfate was found to dominate the total ionic mass (25%) followed by nitrate. In addition, most

aerosol species showed pronounced season variations in the pre-monsoon period due to biomass burning impacts from India and Nepal. Zhao et al. (2013) also characterized the chemical composition and sources of total suspended particulate (TSP) at Lulang on the southeastern TP based on one year measurement. Similar seasonal variations with higher concentrations during pre-monsoon were observed. The back trajectory analysis showed evident transport of air pollutants from south Asia to the TP. The analysis of size-segregated aerosol samples collected at a remote site in the inland Tibetan Plateau during 2012 further confirmed the high concentrations of organic carbon (OC) and elemental carbon (EC) during the pre-monsoon period (Wan et al., 2015), although their concentrations in PM_1 (2.38 and 0.08 μg m^{-3}, respectively) were much lower than those reported in eastern China. Most studies above were conducted in the southeastern Tibetan Plateau. Comparatively, aerosol particles showed quite different behavior in the northeastern Tibetan Plateau. Li et al. (2013) investigated the sources and chemical composition of fine particles collected at a remote site (Qinghai Lake) in the summer of 2010 in the Tibetan Plateau. The average $PM_{2.5}$ concentration was 22±13 μg m^{-3} with sulfate and carbonaceous aerosol being the two major species. Xu et al. (2014b) conducted a year-long measurement of $PM_{2.5}$ composition at the Qilian Shan Station, The annual average concentration of $PM_{2.5}$ was 9.5 ± 5.4 μg m^{-3} with water-soluble ions accounting for 39% of total mass. Water-soluble ions were dominated by sulfate (39%) and showed pronounced seasonal variations. The aerosol composition, size distributions, and back trajectory analysis together indicated a mixed impact of both mineral dust from arid areas of northwest China and anthropogenic emissions from urban areas. However, previous extensive efforts to characterize the chemical properties of aerosol particles in the Tibetan Plateau heavily rely on filter measurements with the duration ranging from days to weeks, real-time measurement of aerosol particle composition is still very limited. A recent study by Xu et al. (2014a) deployed a high-resolution time-of-flight aerosol mass spectrometer (HR-ToF-AMS) at an urban site in Lanzhou in northwest China. The submicron aerosol in the city was dominated by organic aerosol (47%) with a large contribution from local traffic and

cooking emissions (40%). To our knowledge, there is no such real-time measurement of aerosol particle composition with aerosol mass spectrometer at rural sites in the Tibetan Plateau yet.

The study of new particle formation and growth events in the Tibetan Plateau is also relatively new. Since 2004, a number of studies have been conducted to investigate the new particle formation (NPF) and particle growth events in various environments in China (Wu et al., 2007; Wiedensohler et al., 2009; Yue et al., 2010; Zhang et al., 2011b; Wang et al., 2013a; Wang et al., 2013b). The NPF events were frequently observed in urban cities, rural sites, coastal regions, and mountain sites. Sulfuric acid was found to play a dominant role in both NPF and subsequent particle growth, while organics makes an important contributor to particle growth (Yue et al., 2010). The particle growth rates varied largely depending on sites and days, yet generally fell within 1 – 20 nm hr^{-1}. Kivekas et al. (2009) conducted a long-term measurement of particle number size distributions at Waliguan, a regional background site located approximately 140 km southwest of our sampling site. The annual average particle number concentration was found to be higher than other rural sites in the world. Despite this, the particle growth and its relationship to chemical species in the Tibetan Plateau are rarely investigated and remain poorly understood.

In this study, an Aerodyne Aerosol Chemical Speciation Monitor (ACSM) was first deployed at a national background monitoring site (Menyuan, Qinghai) in the Tibetan Plateau for the real-time characterization of submicron aerosol composition including organics, sulfate, nitrate, ammonium, and chloride from 5 September to 15 October, 2013. Collocated measurements including black carbon and particle number size distributions were also conducted at the same site. Here we report the aerosol composition and variations of submicron aerosols and investigate the sources of organic aerosol with positive matrix factorization (PMF). In addition, the particle growth events are also characterized and the roles of chemical species in particle growth are elucidated.

2 Experimental method

2.1 Sampling site

The sampling site, i.e., the national atmospheric background monitoring station (NBS) (37º36´30"N, 101º15´26"E, 3295 m a.s.l.) is located on the Daban Mountain in Menyuan, Qinghai province (Fig. 1). The sampling site is characterized by a typical Plateau continental climate with a pleasantly cool and short summer, and a long cold winter. The annual average temperature is -1~-2^{o}C, and the precipitation is 426 - 860 mm. In this study, ambient temperature averaged 4.9 ^{o}C (-8.7 - 17.9^{o}C) and wind speed varied largely with an average value of 3 m s^{-1}. In addition, several precipitation events were also observed, particularly during the first half period of this study (Fig. 3). The diurnal profiles of meteorological conditions including temperature, relative humidity, wind speed, and wind direction are shown in Fig. S1. The sampling site is relatively pristine with most areas covered by typical Tibetan Plateau plants, e.g., potentilla fruticosa and kobresia etc. There are no strong local anthropogenic source emissions in this area (~ 741 km^2 with a population of ~2000) except occasional biomass burning events that were observed during this study. The capital city Xining of Qinghai province with a population of 2,290,000 is approximately 160 km south of the sampling site which is connected by a national road G227 with few traffic vehicles.

2.2 Instrumentation

The field measurements were conducted from 5 September to 15 October 2013. All the instruments were placed in an air-conditioned room with the temperature maintaining at ~23 ^{o}C. The chemical compositions of non-refractory submicron aerosol (NR-PM_1) species including organics (Org), sulfate (SO_4), nitrate (NO_3), ammonium (NH_4) and chloride (Cl) were measured *in-situ* by an Aerodyne ACSM (Ng et al., 2011b). A $PM_{2.5}$ cyclone (Model: URG-2000-30ED) was supplied in front of the sampling line to remove coarse particles larger than 2.5 μm. The ambient air was drawn inside the room through a 1/2 inch (outer diameter) stainless steel tube using an external pump (flow rate is ~3 L min^{-1}). The sampling height is approximately 2 m, and the particle residence time in the sampling tube is ~ 5s. A silica gel diffusion dryer was then used to dry aerosol particles before sampling into

the ACSM. After passing through a 100 μm critical orifice, aerosol particles between 30 nm – 1 μm are focused into a narrow particle beam via the aerodynamic lens in the vacuum chamber, and then flash vaporized and ionized at a heated surface (~600^{o}C). The positive ions generated are finally analyzed by a commercial quadrupole mass spectrometer. In this study, the mass spectrometer of ACSM was operated at a scanning rate of 500 ms amu^{-1} from *m/z* 10 to 150. The time resolution is approximately 15 min by alternating 6 cycles between the ambient air and particle-free air. The detailed operation of ACSM has been given in Sun et al.(2012).

In addition to ACSM measurements, a Scanning Mobility Particle Sizer (TSI, 3936) equipped with a long Differential Mobility Analyzer (DMA) was simultaneously operated to measure the particle number size distributions between 11.8 nm – 478.3 nm at a time resolution of 5 min. Other collocated species included CO, O_3, NO_x, and SO_2 by various gas analyzers from Thermo Scientific and black carbon (BC) by an Aethalometer (AE31, Magee Scientific Corp.). The meteorological parameters, e.g., temperature, relative humidity, pressure, visibility, precipitation, wind speed and wind direct were also recorded at the same site. All the data are reported with ambient conditions at Beijing Standard Time.

2.3 Data analysis

The ACSM data were analyzed within Igor Pro (WaveMetrics, Inc., Oregon USA) using the standard ACSM data analysis software (v.1.5.3.0). The mass concentrations and chemical composition of NR-PM_1 species were obtained using the default relative ionization efficiency (RIE) that is 1.4, 1.2, 1.1 and 1.3 for organics, sulfate, nitrate and chloride, respectively, except ammonium (6.5) that was derived from pure ammonium nitrate during ionization efficiency (IE) calibration. A collection efficiency (CE) of 0.5 was used to account for the incomplete detection of aerosol species (Matthew et al., 2008; Middlebrook et al., 2012) because aerosol particles were dry and only slightly acidic, and also the mass fraction of ammonium nitrate is not high enough to affect CE significantly.

The sources of organic aerosol were investigated by performing Positive Matrix Factorization (PMF2.exe, v 4.2) on ACSM OA mass spectra (Paatero and Tapper,

1994; Ulbrich et al., 2009). PMF is a standard multivariate factor analysis model broadly used in the field of air pollution source apportionment. The detailed PMF analysis of organic aerosol from AMS measurements, including error matrix preparation, data pretreatment, selections of the optimum number of factors and rotational forcing parameter (FPEAK), and the evaluation of PMF solutions was given in Ulbrich et al. (2009) and Zhang et al. (2011a). In this study, the organic mass spectra from *m/z* 12 to *m/z* 125 were used for the PMF analysis. Because of the absence of collocated measurements, the two factor solution with fpeak = 0 and Q/Q_{exp} close to 1 was chosen (see Fig. S2 for the PMF diagnostic plots). The two factors including a biomass burning OA (BBOA) and an oxygenated OA (OOA) were identified. The two OA factors showed largely different factor profiles and time series indicating their distinct sources.

3 Results and discussion

3.1 Mass concentration and chemical composition of submicron aerosol

Figure 2 shows a comparison of the total PM_1 mass (NR-PM_1 + BC) with that determined from the SMPS measurements. Assuming spherical particles, the SMPS number concentrations were converted to the mass concentrations using chemically-resolved particle density that was estimated from the chemical composition of PM_1 (Salcedo et al., 2006). As shown in Fig. 2, the time series of PM_1 tracks well with that of SMPS measurements (r^2 = 0.87). The slope of 0.52 is likely due to the limited size range of SMPS measurements (12 – 478 nm) by missing a considerable fraction of large particles that ACSM can measure. The PM_1 mass varied dramatically throughout the study with hourly average concentration ranging from 1.0 to 78.4 μg m^{-3}. The average mass concentration of PM_1 (±1σ) for the entire study is 11.9 (± 8.5) μg m^{-3}, which is ~3 – 4 times lower than those observed at rural sites in China (29.9 – 44.1 μg m^{-3}) (Huang et al., 2011; Hu et al., 2013; Huang et al., 2013; Zhang et al., 2014). It is also approximately twice lower than that (24.5 μg m^{-3}) measured at an urban site in Lanzhou in the Tibetan Plateau (Xu et al., 2014a). While the average PM_1 mass concentration in this study is close to those observed at the remote sites in Asia, e.g., Okinawa (14.5 μg m^{-3}) (Zhang et al., 2007a) and Fukue

(12.0 μg m^{-3}) (Takami et al., 2005) in Japan, and Jeju (8.6 μg m^{-3}) in Korea (Topping et al., 2004), it is much higher than those reported at rural/remote sites in north America and Europe, e.g., Chebogue (2.9 μg m^{-3}), Storm Peak (2.1 μg m^{-3}) and Hyytiala (2.0 μg m^{-3}), and even comparable to the loadings at urban sites, e.g., New York City (12 μg m^{-3}), Pittsburgh (15 μg m^{-3}), Manchester (14.0 μg m^{-3}) (Zhang et al., 2007a). These results suggest that the NBS is a typical rural site in Asia, yet with higher background concentrations compared to those in other continents.

Figure 3 shows the time series of mass concentrations and mass fractions of aerosol species in PM_1. The average PM_1 composition is dominated by organics and sulfate on average accounting for 43% and 28%, respectively. Black carbon and chloride represent small fractions contributing 4.5% and 1.2%, respectively to PM_1. As shown in Fig. 1, the aerosol composition at the NBS is largely different from that observed at the urban site in the Tibetan Plateau (Xu et al., 2014a). In particular, sulfate shows ~60% higher contribution, yet BC is more than twice lower than that observed at the urban site (Fig. 1). Xu et al. (2014a) found that 47% of BC was from local traffic emissions which well explained the higher contribution of BC at the urban site. Compared to this study, the average composition of PM_1 measured by the AMS at other rural sites in China showed similar dominance of sulfate (25 – 34%) except Changdao Island (19%), yet overall higher contributions of nitrate because most these rural sites are close to urban areas with high NO_x emissions. The sulfate contributions become more dominant (36 – 64%) at remote sites in East Asia which are far away from urban areas. The increase of sulfate contribution is associated with a large reduction of nitrate contribution (< 5%). Such a change in aerosol bulk composition at rural/remote sites in East Asia is shown Fig. 1. Overall, organics comprises the major fraction of PM_1, contributing approximately one third of the total mass at most sites. While sulfate plays a dominant role in PM_1 at remote sites, nitrate shows the highest contribution at the rural sites in eastern China. Such compositional differences illustrate the different sources of sulfate and nitrate. While sulfate is dominantly from regional sources and transport, nitrate is more likely influenced by anthropogenic NO_x emissions over a smaller regional areas.

Aerosol species also varied dramatically throughout the study. For example, the organics increased rapidly from 2.9 μg m^{-3} to 77.8 μg m^{-3} in one hour on 21 September. While sulfate remained small variations, nitrate, chloride, and BC showed similar steep increases as organics indicating strong impacts of local biomass burning (Zhang et al., 2015). Rapid decreases of aerosol species due to the precipitation of scavenging or wind direction change were also frequently observed. For a better understanding aerosol composition under variable meteorological conditions and sources, five episodes with two of them from clean periods are shown in Fig. 3d. The aerosol composition varied largely among different episodes. While the average PM_1 mass concentrations during the two clean episodes are similar (3.6 and 3.8 μg m^{-3}), the episode of Clean2 shows much higher contribution of organics (48% vs. 34%) with slightly lower sulfate (33% vs. 36%) than Clean 1, consistent with their different air mass trajectories (Fig. S3). The other three episodes show ~5 – 8 times higher mass concentration of PM_1 (17.6 – 27.2 μg m^{-3}) than the two clean episodes. The Ep1 is dominated by organics (70%), almost twice of those during the other two episodes suggesting a largely different source. The relative contributions of sulfate and organics during Ep2 and Ep3 are different although the nitrate contribution is similar. These results suggest that the national background site is subject to the influences of air masses from different sources, some of which are enriched with OA while others are dominated with aerosols mainly composed of ammonium sulfates. We also noticed that the two clean periods showed overall higher contribution of sulfate and lower contribution of nitrate compared to the three pollution episodes. The possible reasons were likely due to that the air masses during clean periods were either from a longer transport when ammonium nitrate was deposited or evaporated due to dilution processes, or from less anthropogenic influenced regions with low NO_x emissions.

The aerosol particle acidity was evaluated using the ratio of measured NH_4^+ ($NH_4^+_{meas}$) to the predicted NH_4^+ ($NH_4^+_{pred}$ = 18×(2×SO_4 /96+NO_3/62+Cl/35.5) that needs to fully neutralize sulfate, nitrate, and chloride (Zhang et al., 2007b). The $NH_4^+_{meas}$ correlates tightly with $NH_4^+_{pred}$ (r^2 = 0.95), yielding a regression slope of 0.80. The results suggest that aerosol particles at the NBS are overall acidic. Similar

acidic particles were also observed at other rural sites in China, e.g., Jiaxing in Yangtze River Delta (Huang et al., 2013), Kaiping in Pearl River Delta (Huang et al., 2011), Yufa in Beijing (Takegawa et al., 2009), and Qilianshan Mountain in the northeast of the Qinghai–Xizang Plateau (Xu et al., 2015). As a comparison, the aerosol particles in the urban city Lanzhou in the Tibetan Plateau were overall neutralized (Xu et al., 2014a). One of the explanations is that more SO_2 is oxidized to sulfate during the transport while gaseous ammonia is not enough to neutralize the newly formed sulfate. This is supported by the overall higher contribution of sulfate at rural/remote sites than that at urban sites. Also note that the newly formed sulfate particles during the frequent NPF events might also have played a role.

3.2 Diurnal variations

The diurnal cycles of aerosol species and PM_1 are shown in Fig. 4a. The PM_1 shows a pronounced diurnal cycle with the concentration ranging from 7.9 to 13.4 μg m^{-3}. The PM_1 shows a visible peak at noon time and then has a gradual decrease reaching the minimum approximately at 16:00. After that, the PM_1 starts to build up and reaches the highest level at midnight. Such a diurnal cycle is similar to those of SO_2 and CO (Fig. 4d), which likely indicates that the major source of PM_1 at the NBS is from regional transport. All aerosol species present similarly pronounced diurnal cycles to PM_1 with the lowest concentrations occurring approximately at 16:00, indicating that the diurnal cycles of aerosol species were mainly driven by the dynamics of planetary boundary layer. Organics dominated PM_1 composition throughout the day varying from 38% - 51%. The concentration of organics at 16:00 is approximately twice lower than that at midnight. Sulfate shows the largest noon peak among all aerosol species, consistent with those of SO_2 and CO. The sulfate contributes more than 25% to PM_1 with the highest contribution as much as 33% between 12:00 – 14:00. Nitrate and chloride shows relatively stable concentrations before 11:00 and then gradually decreased to low ambient levels during daytime. Such diurnal variations still exist after considering the dilution effects of boundary layer height using the conserved tracer CO as a reference (Fig. 4c). This indicates that gas-particle partitioning affected by temperature and humidity has played an

317 important role in driving the diurnal variations of nitrate and chloride. Consistently,
318 the nitrate contribution to PM_1 during late afternoon is ~7-8% which is much lower
319 than that (> 12%) in the early morning. The diurnal variation of BC is different from
320 that observed at the urban site in the Tibetan Plateau where the pronounced morning
321 peak due traffic influences was observed (Xu et al., 2014a). In fact, BC has a good
322 correlation with secondary nitrate (r^2 = 0.59) indicating that BC is likely dominantly
323 from regional transport. This is also supported by the low ambient levels of NO_x (2.5
324 – 5.1 μg m^{-3}). The contribution of BC to PM_1 is relatively constant, which is ~ 4 – 5%
325 throughout the day.

326 **3.3 OA composition and sources**

327 PMF analysis of ACSM OA mass spectra identified two factors, i.e., a biomass
328 burning OA (BBOA) and an oxygenated OA (OOA). The mass spectra and time
329 series of the two OA factors are shown in Fig. 5.

330 **3.3.1 BBOA**

331 The mass spectrum of BBOA resembles to that of standard BBOA (r^2 = 0.82)
332 which is characterized by a prominent peak of *m/z* 60 (1.1% of total signal), a tracer
333 *m/z* for biomass burning aerosols (Aiken et al., 2009; Cubison et al., 2011; Hennigan
334 et al., 2011). The fraction of *m/z* 60 in BBOA (1.1%) is also much higher than ~0.3%
335 in the absence of biomass burning impacts (Cubison et al., 2011). BBOA correlates
336 tightly with *m/z* 60 (r^2 = 0.82) and also chloride (r^2 = 0.52). The ratio of BBOA to *m/z*
337 60 is 55.6, which is higher than that of fresh BBOA (34.5) measured during the
338 second Fire Lab at Missoula Experiment (FLAME II) (Lee et al., 2010). One of the
339 explanations is that BBOA in the ambient is more aged because the *m/z* 60 related
340 levoglucosan can be rapidly oxidized in the atmosphere (Hennigan et al., 2010).
341 Indeed, Zhang et al. (2015) reported a much higher ratio of aged BBOA to *m/z* 60
342 (74.8) than fresh BBOA (16.8) during two harvest seasons in Nanjing, China. The
343 time series of BBOA shows periodically large peaks, particularly on the days of 21
344 and 22 September, which were mainly from the burning of a large amount of straws in
345 the south-west region. Relatively high concentration of BBOA was also observed at
346 the end of the campaign due to the burning of cow dung for heating purpose because

of the low temperature. The average concentration of BBOA is 0.8 (± 1.5) μg m^{-3} for the entire study on average accounting for 15% of total OA. Although the average BBOA contribution is much lower than those measured in PRD, e.g., Jiaxing (~3.9 μg m^{-3}, 30.1%) (Huang et al., 2013), Kaiping (~1.36 μg m^{-3}, 24.5%) (Huang et al., 2011), and Shenzhen (~5.2 μg m^{-3}, 29.5%) (He et al., 2011), the contribution of BBOA during some strong BB plumes can reach up to 40%, e.g., 21-22 September, indicating a large impact of biomass burning on OA at the national background site. BBOA showed a pronounced diurnal cycle which is similar to that of chloride (Fig. 5c). The BBOA concentration increased rapidly from 18:00 and reached a maximum in 2 hours, likely indicating that the burning of straws and cow dung mainly occurred during this period of time. As a result, the contribution of BBOA to total OA increased from ~10% to more than 20%.

3.3.2 Oxygenated organic aerosols (OOA)

Similar to previously reported OOA (Zhang et al., 2005), the mass spectrum of OOA in this study is characterized by a prominent *m/z* 44 peak (mainly CO_2^+). The mass spectrum of OOA also resembles to that of low-volatility OOA (r^2 = 0.88) (Ng et al., 2011a), yet with higher fraction of *m/z* 44 (f_{44}). Much higher fraction of *m/z* 44 in ACSM OOA spectrum than that from HR-ToF-AMS was reported recently by a comprehensive evaluation of the ACSM (Fröhlich et al., 2015). The results also showed that f_{44} has minor impacts on the mass concentrations of OOA factors, although it varies largely by a factor of 0.6 – 1.3. The average mass concentration of OOA is 4.1 μg m^{-3}, on average accounting for 85% of total OA. The OOA contribution is much higher than those reported at urban sites in summer (~60%) (Huang et al., 2010; Sun et al., 2012; Xu et al., 2014a), and also higher than those (~70%) observed at rural sites in China (Hu et al., 2013; Huang et al., 2013). These results suggest that organic aerosol was highly aged and well processed at the NBS. In addition, aqueous-processing of OA at nighttime associated with high RH might also played a role in forming the highly oxidized OA. The diurnal cycle of OOA was similar to that of PM_1, which showed a small peak before noon time followed by a subsequent decrease until 16:00. The OOA dominated OA throughout the day varying

from 80 – 90%, indicating that OA at the NBS was mainly composed of secondary organic aerosol.

Previous studies have shown the ubiquitously tight correlations between sulfate and highly oxidized OA because of their similar secondary nature over regional scales (Zhang et al., 2005; DeCarlo et al., 2010). While the OOA correlates well with secondary sulfate for most of the time in this study, several periods with largely different correlations were also observed (Fig. 6). As shown in Fig. 5b and 6, the weak correlation events mainly occurred during periods with strong biomass burning impacts were observed. However, it cannot be resolved by extending PMF solution to more than 2 factors because of the limitation of PMF technique in source apportionment analysis. Similar different correlations between sulfate and LV-OOA were also observed during two research flights in Mexico City and the Central Mexican Plateau (DeCarlo et al., 2010). Following the approach suggested by DeCarlo et al. (2010), we performed a post-processing technique with external tracers on the further apportionment of OOA. We first assume that OOA and sulfate have similar sources during periods in the absence of biomass burning impacts, which is supported by their tight correlations ($r^2 = 0.74$). An average OOA/SO_4 ratio of 1.04, i.e., $(OOA/SO_4)_{NBB}$, was obtained by performing a linear regression analysis on OOA versus SO_4. We then assume that SO_4 is completely from non-biomass burning (NBB) sources during BB-impact periods. This assumption is rational because previous studies have found that fresh biomass burning emits a very small or negligible fraction of sulfate (Levin et al., 2010). The sulfate-related OOA can be calculated as $OOA\times [OOA/SO_4]_{NBB}$, and the excess OOA that is from different sources is then determined as:

$$OOA_{post\text{-}processed} = OOA - SO_4\times [OOA/SO_4]_{NBB} \quad (1)$$

Because the post-processed OOA shows high concentrations during BB periods, we conclude that it's very likely an aged BBOA that was mixed with OOA. In fact, the mass spectrum of $OOA_{post\text{-}processed}$ is similar to that of OOA. The fraction of *m/z* 60 (f_{60}) is 0.29%, which is very close to ~0.3% for non-biomass burning organic aerosol (Aiken et al., 2008). Smog chamber experiments have shown that fresh BBOA can be

rapidly oxidized within 3 – 4.5 hours (Hennigan et al., 2011). While f_{44} increases significantly, f_{60} quickly decreases to a value close to ~0.3%. Similarly, a recent study in Nanjing resolved an aged BBOA factor with its spectrum resembling to that of OOA yet with much lower f_{60} (Zhang et al., 2015). The average concentration of aged BBOA is 0.82 (± 2.65) μg m^{-3}, accounting for 17% of OA for the entire study. The contribution of aged BBOA is close to that of fresh BBOA, which might indicate that half of BBOA has been aged. Still, the sum of fresh and aged BBOA highly correlates with *m/z* 60 (r^2 = 0.81, slope = 136.1). The fresh and aged BBOA together accounted for 33% of the total OA suggesting that BBOA was a large local source of OA during the observational period. With the post-processing technique, the sulfate-related OOA contributed 67% on average of total OA, which is close to those observed at other rural sites in e.g., Kaiping (Huang et al., 2011) and Changdao (Hu et al., 2013).

3.4 Chemistry of particle growth

Figure 7a shows the evolution of size distributions of particle number concentrations for the entire study. New particle formation and growth events (NPE) were observed almost every day (27 days in 34 days). Most NPE started at ~11:00 (The time of sunrise is 2 hours behind of Beijing standard time) and persisted more than half day except some NPE were interrupted by either precipitation events or strong winds. The average particle number size distributions during NPE and non event days (non-NPE) are shown in Fig. 7b. Both NPE and non-NPE show broad size distributions with higher number concentrations occurring during NPE. Three modes with geometric mean diameter (GMD) peaking at 28 nm, 43 nm, and 104 nm, respectively were resolved using a log-normal distribution fitting (Seinfeld and Pandis, 2006). The largest mode (104 nm) dominated the total number of particles accounting for ~70%. In contrast, the average size distribution during non-NPE was characterized by a bi-modal distribution with the GMD peaking at 59 nm and 146 nm, respectively. The peak diameters were shifted to the larger sizes compared to those during NPE. Such a size shift from clean days to polluted days was also observed previously in Beijing (Yue et al., 2010). Also, the two modes showed almost equivalent contributions to the total number of particles. The average particle number

concentration for the entire study is 2.4 × 10^3 cm^{-3}, which is nearly an order of magnitude lower than those reported at rural sites in eastern China (Wu et al., 2007), but close to that (2.03×10^3 cm^{-3}) observed at Mount Waliguan which is a remote site located nearby (Kivekas et al., 2009). The particle size was further segregated into small Aitken mode (20 – 40 nm, $N_{20\text{-}40}$), large Aitken mode (40 – 100 nm, $N_{40\text{-}100}$), and Accumulation mode (100 – 470 nm, N_{Accu}) particles. The time series and diurnal cycles of particle numbers for three different sizes are shown in Fig. 7c, d. The $N_{20\text{-}40}$ presented sharp peaks almost in everyday corresponding to new particle formation events. The diurnal cycle of $N_{20\text{-}40}$ showed that the number concentration started to increase at approximately 11:00 (150 cm^{-3}) and reached a maximum at 14:00 (770 cm^{-3}). In contrast, the $N_{40\text{-}100}$ and N_{Accu} showed largely different diurnal cycles from that of $N_{20\text{-}40}$, indicating their different sources. In fact, the diurnal cycles of $N_{40\text{-}100}$ and N_{Accu} are remarkably similar to those of aerosol species, suggesting that the large particles are more likely from regional transport.

Figure 8 shows the diurnal evolution of particle number size distributions, aerosol composition, and gaseous species during NPE and non-NPE days. The particle number size distributions during NPE were characterized by distinct bimodal distributions showing a persistent larger mode with the GMD peaking at ~100 nm, and a smaller mode below 50 nm. The particle growth started at approximately 11:00 from ~20 nm, and continued to grow slowly until ~45 nm at mid-night. The maximum size particles can grow in this study is generally smaller than those (~60 – 70 nm) observed at urban and rural sites in Beijing (Wang et al., 2013a), which is likely due to the much lower concentrations of aerosol species and precursors. All aerosol species however showed decreases during the particle growth period between 12:00 – 17:00, and the gaseous CO and SO_2 showed similar variations as aerosol species. By excluding the dilution effect of PBL using CO as a tracer, we found that organics was the only species showing a gradual increase during the particle growth period (Fig. 8a) while other species remained minor changes or even slightly decreased. The contribution of organics to PM_1 also showed a corresponding increase from 40% to 47%. These results suggest that organics might have played a dominant role in

particle growth at the national background site. Our conclusion is consistent with the recent findings that organics, particularly oxidized organic aerosol species, play a more important role than ammonium sulfate in particle growth (Dusek et al., 2010; Ehn et al., 2014; Setyan et al., 2014). Also note that the contribution of organics to PM_1 during NPE (~40 – 50%) is overall higher than that during non-NPE (~30 – 40%), while the sulfate contribution is correspondingly lower (~20 – 30% vs. 30 – 40%), which further supports the important role of organics during NPE. The particle growth was mixed with anthropogenic sources from 17:00 which are indicated by synchronous enhancements of both aerosol species and gaseous precursors. One of possible reasons is due to the air mass transport from downwind urban areas.

The diurnal evolution of particle size distributions and aerosol composition during non-NPE is largely different from that during NPE. The particle number size distributions and mass concentrations of aerosol species showed a dramatic variation at noon time (12:00), indicating a very different chemical and/or physical process between the first and the second half day. The aerosol particles showed an evident growth from ~50 nm to 60 nm during the first 6 hours, which is likely a continuation of previous NPE. Compared to the early stage of particle growth during NPE, the particle growth during non-NPE is associated with synchronous increases of both organics and sulfate. The results indicate that both organics and sulfate contribute to the particle growth after mixed with anthropogenic sources from ~18:00 in the previous day.

We further calculated the particle growth rates (GR) for NPE events without interruptions due to meteorological changes using Eq. (2).

$$GR = \frac{\Delta D_m}{\Delta t} \qquad (2)$$

where D_m is the geometric mean diameter from the log-normal fitting, ΔD_m is the difference of diameter during the growth period and Δt is the duration of growth time. The calculated GR and the corresponding average chemical composition and fraction of OOA during the growth period are shown in Fig. 9a. The GR ranges from 0.8 nm h^{-1} to 3.2 nm h^{-1} with an average of 2.0 nm h^{-1}. The GR in this study is overall

consistent with those observed at remote and/or forest sites (Eisele and McMurry, 1997; Weber et al., 1997), yet generally smaller than those measured at urban and polluted rural sites (Yue et al., 2010; Shen et al., 2011; Zhang et al., 2011b) where abundant condensable vapor and high concentrations of particulate matter facilitate the growth of particles (Wang et al., 2013a). By linking GR to aerosol composition, we found that GR at the background site is positively related to the fraction of oxidized OA, which likely indicate the important role of oxidized secondary organic aerosol in particle growth (Ehn et al., 2014). Zhang et al. (2011b) also observed a tight correlation between OOA and GR in urban Beijing supporting the important role of OOA in particle growth. Further investigation is needed for a better understanding of the role of organic aerosol, particularly oxidized OA, in the new particle formation and particle growth at the regional background site.

4 Conclusions

The aerosol particle composition and particle number size distributions were measured at a national background monitoring station in the Tibetan Plateau (3295 m, a.s.l.) from 5 September to 15 October 2013. The average mass concentration of PM_1 is 11.4 (± 8.5) μg m^{-3} for the entire study, which is lower than those observed at urban and rural sites in eastern China. Organics constituted the major fraction of PM_1, on average accounting for 43% followed by sulfate (28%) and ammonium (11%). Several periods with the contribution of organics as much as 70% due to biomass burning impacts were also observed. All aerosol species presented similar diurnal cycles that were mainly driven by the dynamics of planetary boundary layer and regional transport. PMF source apportionment analysis resolved a secondary OOA and a primary BBOA. OOA dominated OA composition accounting for 85% on average with the rest being BBOA. A post-processing technique based on the correlation of OOA and sulfate separated an aged BBOA which on average accounted for 17% of OA. New particle formation and particle growth events were frequently observed during this study. The particle growth rates varied from 0.8 to 3.2 nm hr^{-1} with an average growth rate of 2.0 nm hr^{-1}. Organics was found to be the only species with gradually increased contribution to PM_1 during NPE. Also, higher contribution

of organics during NPE than non-NPE days was observed. These results potentially illustrate the important role of organics in particle growth. Further analysis showed a positive correlation of particle growth rate with the fraction of OOA suggesting that oxidized OA plays a critical role contributing to the particle growth.

Acknowledgements

This work was supported by the National Natural Science Foundation of China (41375133), the National Key Project of Basic Research (2013CB955801), and the Strategic Priority Research Program (B) of the Chinese Academy of Sciences (Grant No. XDB05020500). We thank the National Station for Background Atmospheric Monitoring for providing the meteorological data and gaseous data.

References

Aiken, A. C., DeCarlo, P. F., Kroll, J. H., Worsnop, D. R., Huffman, J. A., Docherty, K. S., Ulbrich, I. M., Mohr, C., Kimmel, J. R., Sueper, D., Sun, Y., Zhang, Q., Trimborn, A., Northway, M., Ziemann, P. J., Canagaratna, M. R., Onasch, T. B., Alfarra, M. R., Prevot, A. S. H., Dommen, J., Duplissy, J., Metzger, A., Baltensperger, U., and Jimenez, J. L.: O/C and OM/OC ratios of primary, secondary, and ambient organic aerosols with High-Resolution Time-of-Flight Aerosol Mass Spectrometry, Environ. Sci. Technol., 42, 4478-4485, 2008.

Aiken, A. C., Salcedo, D., Cubison, M. J., Huffman, J. A., DeCarlo, P. F., Ulbrich, I. M., Docherty, K. S., Sueper, D., Kimmel, J. R., Worsnop, D. R., Trimborn, A., Northway, M., Stone, E. A., Schauer, J. J., Volkamer, R. M., Fortner, E., de Foy, B., Wang, J., Laskin, A., Shutthanandan, V., Zheng, J., Zhang, R., Gaffney, J., Marley, N. A., Paredes-Miranda, G., Arnott, W. P., Molina, L. T., Sosa, G., and Jimenez, J. L.: Mexico City aerosol analysis during MILAGRO using high resolution aerosol mass spectrometry at the urban supersite (T0) - Part 1: Fine particle composition and organic source apportionment, Atmos. Chem. Phys., 9, 6633-6653, 2009.

Cao, J., Lee, S., Chow, J. C., Watson, J. G., Ho, K., Zhang, R., Jin, Z., Shen, Z., Chen, G., and Kang, Y.: Spatial and seasonal distributions of carbonaceous aerosols over China, J. Geophys. Res., 112, 2007.

Cong, Z., Kang, S., Kawamura, K., Liu, B., Wan, X., Wang, Z., Gao, S., and Fu, P.: Carbonaceous aerosols on the south edge of the Tibetan Plateau: concentrations, seasonality and sources, Atmos. Chem. Phys., 15, 1573-1584, 10.5194/acp-15-1573-2015, 2015.

Cubison, M. J., Ortega, A. M., Hayes, P. L., Farmer, D. K., Day, D., Lechner, M. J., Brune, W. H., Apel, E., Diskin, G. S., Fisher, J. A., Fuelberg, H. E., Hecobian, A., Knapp, D. J., Mikoviny, T., Riemer, D., Sachse, G. W., Sessions, W., Weber, R. J., Weinheimer, A. J., Wisthaler, A., and

563 Jimenez, J. L.: Effects of aging on organic aerosol from open biomass burning smoke in
564 aircraft and laboratory studies, Atmos. Chem. Phys., 11, 12049-12064,
565 10.5194/acp-11-12049-2011, 2011.
566 DeCarlo, P. F., Ulbrich, I. M., Crounse, J., de Foy, B., Dunlea, E. J., Aiken, A. C., Knapp, D.,
567 Weinheimer, A. J., Campos, T., Wennberg, P. O., and Jimenez, J. L.: Investigation of the
568 sources and processing of organic aerosol over the Central Mexican Plateau from aircraft
569 measurements during MILAGRO, Atmos. Chem. Phys., 10, 5257-5280,
570 10.5194/acp-10-5257-2010, 2010.
571 Dusek, U., Frank, G. P., Curtius, J., Drewnick, F., Schneider, J., Kürten, A., Rose, D., Andreae, M.
572 O., Borrmann, S., and Pöschl, U.: Enhanced organic mass fraction and decreased
573 hygroscopicity of cloud condensation nuclei (CCN) during new particle formation events,
574 Geophys. Res. Lett., 37, L03804, 10.1029/2009gl040930, 2010.
575 Ehn, M., Thornton, J. A., Kleist, E., Sipila, M., Junninen, H., Pullinen, I., Springer, M., Rubach,
576 F., Tillmann, R., Lee, B., Lopez-Hilfiker, F., Andres, S., Acir, I.-H., Rissanen, M., Jokinen, T.,
577 Schobesberger, S., Kangasluoma, J., Kontkanen, J., Nieminen, T., Kurten, T., Nielsen, L. B.,
578 Jorgensen, S., Kjaergaard, H. G., Canagaratna, M., Maso, M. D., Berndt, T., Petaja, T.,
579 Wahner, A., Kerminen, V.-M., Kulmala, M., Worsnop, D. R., Wildt, J., and Mentel, T. F.: A
580 large source of low-volatility secondary organic aerosol, Nature, 506, 476-479,
581 10.1038/nature13032, 2014.
582 Eisele, F. L., and McMurry, P. H.: Recent progress in understanding particle nucleation and
583 growth, Philosophical Transactions of the Royal Society B: Biological Sciences, 352,
584 191-201, 10.1098/rstb.1997.0014, 1997.
585 Fröhlich, R., Crenn, V., Setyan, A., Belis, C. A., Canonaco, F., Favez, O., Riffault, V., Slowik, J. G.,
586 Aas, W., Aijälä, M., Alastuey, A., Artiñano, B., Bonnaire, N., Bozzetti, C., Bressi, M.,
587 Carbone, C., Coz, E., Croteau, P. L., Cubison, M. J., Esser-Gietl, J. K., Green, D. C., Gros, V.,
588 Heikkinen, L., Herrmann, H., Jayne, J. T., Lunder, C. R., Minguillón, M. C., Močnik, G.,
589 O'Dowd, C. D., Ovadnevaite, J., Petralia, E., Poulain, L., Priestman, M., Ripoll, A.,
590 Sarda-Estève, R., Wiedensohler, A., Baltensperger, U., Sciare, J., and Prévôt, A. S. H.:
591 ACTRIS ACSM intercomparison – Part 2: Intercomparison of ME-2 organic source
592 apportionment results from 15 individual, co-located aerosol mass spectrometers, Atmos.
593 Meas. Tech. Discuss., 8, 1559-1613, 10.5194/amtd-8-1559-2015, 2015.
594 Gong, Z., Lan, Z., Xue, L., Zeng, L., He, L., and Huang, X.: Characterization of submicron
595 aerosols in the urban outflow of the central Pearl River Delta region of China, Front.
596 Environ. Sci. Eng., 10.1007/s11783-012-0441-8, 2012.
597 He, L.-Y., Huang, X.-F., Xue, L., Hu, M., Lin, Y., Zheng, J., Zhang, R., and Zhang, Y.-H.: Submicron
598 aerosol analysis and organic source apportionment in an urban atmosphere in Pearl
599 River Delta of China using high-resolution aerosol mass spectrometry, J. Geophys. Res.,
600 116, 10.1029/2010jd014566, 2011.
601 Hennigan, C. J., Sullivan, A. P., Collett, J. L., and Robinson, A. L.: Levoglucosan stability in
602 biomass burning particles exposed to hydroxyl radicals, Geophys. Res. Lett., 37, L09806,
603 doi:10.1029/2010GL043088, 2010.
604 Hennigan, C. J., Miracolo, M. A., Engelhart, G. J., May, A. A., Presto, A. A., Lee, T., Sullivan, A.
605 P., McMeeking, G. R., Coe, H., Wold, C. E., Hao, W. M., Gilman, J. B., Kuster, W. C., de
606 Gouw, J., Schichtel, B. A., Collett, J. L., Kreidenweis, S. M., and Robinson, A. L.: Chemical

and physical transformations of organic aerosol from the photo-oxidation of open biomass burning emissions in an environmental chamber, Atmos. Chem. Phys., 11, 7669-7686, 10.5194/acp-11-7669-2011, 2011.

Hu, W. W., Hu, M., Yuan, B., Jimenez, J. L., Tang, Q., Peng, J. F., Hu, W., Shao, M., Wang, M., Zeng, L. M., Wu, Y. S., Gong, Z. H., Huang, X. F., and He, L. Y.: Insights on organic aerosol aging and the influence of coal combustion at a regional receptor site of central eastern China, Atmos. Chem. Phys., 13, 10095-10112, 10.5194/acp-13-10095-2013, 2013.

Huang, X.-F., Xue, L., Tian, X.-D., Shao, W.-W., Sun, T.-L., Gong, Z.-H., Ju, W.-W., Jiang, B., Hu, M., and He, L.-Y.: Highly time-resolved carbonaceous aerosol characterization in Yangtze River Delta of China: composition, mixing state and secondary formation, Atmos. Environ., 64, 200 - 207, 10.1016/j.atmosenv.2012.09.059, 2013.

Huang, X. F., He, L. Y., Hu, M., Canagaratna, M. R., Sun, Y., Zhang, Q., Zhu, T., Xue, L., Zeng, L. W., Liu, X. G., Zhang, Y. H., Jayne, J. T., Ng, N. L., and Worsnop, D. R.: Highly time-resolved chemical characterization of atmospheric submicron particles during 2008 Beijing Olympic Games using an Aerodyne High-Resolution Aerosol Mass Spectrometer, Atmos. Chem. Phys., 10, 8933-8945, 10.5194/acp-10-8933-2010, 2010.

Huang, X. F., He, L. Y., Hu, M., Canagaratna, M. R., Kroll, J. H., Ng, N. L., Zhang, Y. H., Lin, Y., Xue, L., Sun, T. L., Liu, X. G., Shao, M., Jayne, J. T., and Worsnop, D. R.: Characterization of submicron aerosols at a rural site in Pearl River Delta of China using an Aerodyne High-Resolution Aerosol Mass Spectrometer, Atmos. Chem. Phys., 11, 1865-1877, 10.5194/acp-11-1865-2011, 2011.

Huang, X. F., He, L. Y., Xue, L., Sun, T. L., Zeng, L. W., Gong, Z. H., Hu, M., and Zhu, T.: Highly time-resolved chemical characterization of atmospheric fine particles during 2010 Shanghai World Expo, Atmos. Chem. Phys., 12, 4897-4907, 10.5194/acp-12-4897-2012, 2012.

Jacobson, M. Z.: Strong radiative heating due to the mixing state of black carbon in atmospheric aerosols, Nature, 409, 695-697, http://www.nature.com/nature/journal/v409/n6821/suppinfo/409695a0_S1.html, 2001.

Kivekas, N., Sun, J., Zhan, M., Kerminen, V. M., HyvÃ¤rinen, A., Komppula, M., Viisanen, Y., Hong, N., Zhang, Y., Kulmala, M., Zhang, X. C., Deli, G., and Lihavainen, H.: Long term particle size distribution measurements at Mount Waliguan, a high-altitude site in inland China, Atmos. Chem. Phys., 9, 5461-5474, 2009.

Lee, T., Sullivan, A. P., Mack, L., Jimenez, J. L., Kreidenweis, S. M., Onasch, T. B., Worsnop, D. R., Malm, W., Wold, C. E., Hao, W. M., and Collett, J. L.: Chemical Smoke Marker Emissions During Flaming and Smoldering Phases of Laboratory Open Burning of Wildland Fuels, Aerosol Sci. Technol., 44, i-v, 10.1080/02786826.2010.499884, 2010.

Levin, E. J. T., McMeeking, G. R., Carrico, C. M., Mack, L. E., Kreidenweis, S. M., Wold, C. E., Moosmüller, H., Arnott, W. P., Hao, W. M., Collett, J. L., Jr., and Malm, W. C.: Biomass burning smoke aerosol properties measured during Fire Laboratory at Missoula Experiments (FLAME), J. Geophys. Res., 115, D18210, 10.1029/2009jd013601, 2010.

Li, J. J., Wang, G. H., Wang, X. M., Cao, J. J., Sun, T., Cheng, C. L., Meng, J. J., Hu, T. F., and Liu, S. X.: Abundance, composition and source of atmospheric PM 2.5 at a remote site in the Tibetan Plateau, China, Tellus B, 65, 2013.

Matthew, B. M., Middlebrook, A. M., and Onasch, T. B.: Collection efficiencies in an Aerodyne

Aerosol Mass Spectrometer as a function of particle phase for laboratory generated aerosols, Aerosol Sci. Technol., 42, 884-898, 10.1080/02786820802356797, 2008.
Middlebrook, A. M., Bahreini, R., Jimenez, J. L., and Canagaratna, M. R.: Evaluation of Composition-Dependent Collection Efficiencies for the Aerodyne Aerosol Mass Spectrometer using Field Data, Aerosol Sci. Technol., 46, 258-271, 10.1080/02786826.2011.620041, 2012.
Ng, N. L., Canagaratna, M. R., Jimenez, J. L., Zhang, Q., Ulbrich, I. M., and Worsnop, D. R.: Real-time methods for estimating organic component mass concentrations from Aerosol Mass Spectrometer data, Environ. Sci. Technol., 45, 910-916, 10.1021/es102951k, 2011a.
Ng, N. L., Herndon, S. C., Trimborn, A., Canagaratna, M. R., Croteau, P. L., Onasch, T. B., Sueper, D., Worsnop, D. R., Zhang, Q., Sun, Y. L., and Jayne, J. T.: An Aerosol Chemical Speciation Monitor (ACSM) for Routine Monitoring of the Composition and Mass Concentrations of Ambient Aerosol, Aerosol Sci. Technol., 45, 780-794, 10.1080/02786826.2011.560211, 2011b.
Paatero, P., and Tapper, U.: POSITIVE MATRIX FACTORIZATION - A NONNEGATIVE FACTOR MODEL WITH OPTIMAL UTILIZATION OF ERROR-ESTIMATES OF DATA VALUES, Environmetrics, 5, 111-126, 10.1002/env.3170050203, 1994.
Salcedo, D., Onasch, T. B., Dzepina, K., Canagaratna, M., Zhang, Q., Huffman, J., DeCarlo, P., Jayne, J., Mortimer, P., and Worsnop, D. R.: Characterization of ambient aerosols in Mexico City during the MCMA-2003 campaign with Aerosol Mass Spectrometry: results from the CENICA Supersite, Atmos. Chem. Phys., 6, 925-946, 2006.
Seinfeld, J. H., and Pandis, S. N.: Atmos. Chem. Phys.: from Air Pollution to Climate Change, Wiley, John & Sons, Incorporated, New York, 1203 pp., 2006.
Setyan, A., Song, C., Merkel, M., Knighton, W. B., Onasch, T. B., Canagaratna, M. R., Worsnop, D. R., Wiedensohler, A., Shilling, J. E., and Zhang, Q.: Chemistry of new particle growth in mixed urban and biogenic emissions – insights from CARES, Atmos. Chem. Phys., 14, 6477-6494, 10.5194/acp-14-6477-2014, 2014.
Shen, X. J., Sun, J. Y., Zhang, Y. M., Wehner, B., Nowak, A., Tuch, T., Zhang, X. C., Wang, T. T., Zhou, H. G., Zhang, X. L., Dong, F., Birmili, W., and Wiedensohler, A.: First long-term study of particle number size distributions and new particle formation events of regional aerosol in the North China Plain, Atmos. Chem. Phys., 11, 1565-1580, 10.5194/acp-11-1565-2011, 2011.
Sun, J., Zhang, Q., Canagaratna, M. R., Zhang, Y., Ng, N. L., Sun, Y., Jayne, J. T., Zhang, X., Zhang, X., and Worsnop, D. R.: Highly time- and size-resolved characterization of submicron aerosol particles in Beijing using an Aerodyne Aerosol Mass Spectrometer, Atmos. Environ., 44, 131-140, 2010.
Sun, Y. L., Wang, Z., Dong, H., Yang, T., Li, J., Pan, X., Chen, P., and Jayne, J. T.: Characterization of summer organic and inorganic aerosols in Beijing, China with an Aerosol Chemical Speciation Monitor, Atmos. Environ., 51, 250-259, 10.1016/j.atmosenv.2012.01.013, 2012.
Sun, Y. L., Wang, Z. F., Fu, P. Q., Yang, T., Jiang, Q., Dong, H. B., Li, J., and Jia, J. J.: Aerosol composition, sources and processes during wintertime in Beijing, China, Atmos. Chem. Phys., 13, 4577-4592, 10.5194/acp-13-4577-2013, 2013.
Takami, A., Miyoshi, T., Shimono, A., and Hatakeyama, S.: Chemical composition of fine

695 aerosol measured by AMS at Fukue Island, Japan during APEX period, Atmos. Environ.,
696 39, 4913-4924, 2005.
697 Takegawa, N., Miyakawa, T., Kuwata, M., Kondo, Y., Zhao, Y., Han, S., Kita, K., Miyazaki, Y.,
698 Deng, Z., Xiao, R., Hu, M., van Pinxteren, D., Herrmann, H., Hofzumahaus, A., Holland, F.,
699 Wahner, A., Blake, D. R., Sugimoto, N., and Zhu, T.: Variability of submicron aerosol
700 observed at a rural site in Beijing in the summer of 2006, J. Geophys. Res., 114, D00G05,
701 10.1029/2008jd010857, 2009.
702 Tie, X., and Cao, J.: Aerosol pollution in China: Present and future impact on environment,
703 Particuology, 7, 426-431, http://dx.doi.org/10.1016/j.partic.2009.09.003, 2009.
704 Topping, D., Coe, H., McFiggans, G., Burgess, R., Allan, J., Alfarra, M. R., Bower, K., Choularton,
705 T. W., Decesari, S., and Facchini, M. C.: Aerosol chemical characteristics from sampling
706 conducted on the Island of Jeju, Korea during ACE Asia, Atmos. Environ., 38, 2111-2123,
707 10.1016/j.atmosenv.2004.01.022, 2004.
708 Ulbrich, I. M., Canagaratna, M. R., Zhang, Q., Worsnop, D. R., and Jimenez, J. L.:
709 Interpretation of organic components from Positive Matrix Factorization of aerosol mass
710 spectrometric data, Atmos. Chem. Phys., 9, 2891-2918, 2009.
711 Wan, X., Kang, S. C., Wang, Y. S., Xin, J. Y., Liu, B., Guo, Y. H., Wen, T. X., Zhang, G. S., and Cong,
712 Z. Y.: Size distribution of carbonaceous aerosols at a high-altitude site on the central
713 Tibetan Plateau (Nam Co Station, 4730 m a.s.l.), Atmospheric Research, 153, 155-164,
714 10.1016/j.atmosres.2014.08.008, 2015.
715 Wang, Z. B., Hu, M., Sun, J. Y., Wu, Z. J., Yue, D. L., Shen, X. J., Zhang, Y. M., Pei, X. Y., Cheng, Y.
716 F., and Wiedensohler, A.: Characteristics of regional new particle formation in urban and
717 regional background environments in the North China Plain, Atmos. Chem. Phys., 13,
718 12495-12506, 10.5194/acp-13-12495-2013, 2013a.
719 Wang, Z. B., Hu, M., Wu, Z. J., Yue, D. L., He, L. Y., Huang, X. F., Liu, X. G., and Wiedensohler, A.:
720 Long-term measurements of particle number size distributions and the relationships
721 with air mass history and source apportionment in the summer of Beijing, Atmos. Chem.
722 Phys., 13, 10159-10170, 10.5194/acp-13-10159-2013, 2013b.
723 Weber, R. J., Marti, J. J., McMurry, P. H., Eisele, F. L., Tanner, D. J., and Jefferson, A.:
724 Measurements of new particle formation and ultrafine particle growth rates at a clean
725 continental site, J. Geophys. Res., 102, 4375, 10.1029/96jd03656, 1997.
726 Wiedensohler, A., Cheng, Y. F., Nowak, A., Wehner, B., Achtert, P., Berghof, M., Birmili, W., Wu,
727 Z. J., Hu, M., Zhu, T., Takegawa, N., Kita, K., Kondo, Y., Lou, S. R., Hofzumahaus, A.,
728 Holland, F., Wahner, A., Gunthe, S. S., Rose, D., Su, H., and Poschl, U.: Rapid aerosol
729 particle growth and increase of cloud condensation nucleus activity by secondary aerosol
730 formation and condensation: A case study for regional air pollution in northeastern
731 China, J. Geophys. Res.-Atmos., 114, D00g08,10.1029/2008jd010884, 2009.
732 Wu, Z., Hu, M., Liu, S., Wehner, B., Bauer, S., Ma ßling, A., Wiedensohler, A., Petäjä, T., Dal
733 Maso, M., and Kulmala, M.: New particle formation in Beijing, China: Statistical analysis
734 of a 1-year data set, J. Geophys. Res., 112, 10.1029/2006jd007406, 2007.
735 Xu, J., Zhang, Q., Chen, M., Ge, X., Ren, J., and Qin, D.: Chemical composition, sources, and
736 processes of urban aerosols during summertime in northwest China: insights from
737 high-resolution aerosol mass spectrometry, Atmos. Chem. Phys., 14, 12593-12611,
738 10.5194/acp-14-12593-2014, 2014a.

739 Xu, J. Z., Wang, Z. B., Yu, G. M., Qin, X., Ren, J. W., and Qin, D.: Characteristics of water
740 soluble ionic species in fine particles from a high altitude site on the northern boundary
741 of Tibetan Plateau: Mixture of mineral dust and. anthropogenic aerosol, Atmos. Res., 143,
742 43-56, 10.1016/j.atmosres.2014.01.018, 2014b.
743 Xu, J. Z., Zhang, Q., Wang, Z. B., Yu, G. M., Ge, X. L., and Qin, X.: Chemical composition and
744 size distribution of summertime PM2.5 at a high altitude remote location in the
745 northeast of the Qinghai–Xizang (Tibet) Plateau: insights into aerosol sources and
746 processing in free troposphere, Atmos. Chem. Phys., 15, 5069-5081,
747 10.5194/acp-15-5069-2015, 2015.
748 Yue, D. L., Hu, M., Zhang, R. Y., Wang, Z. B., Zheng, J., Wu, Z. J., Wiedensohler, A., He, L. Y.,
749 Huang, X. F., and Zhu, T.: The roles of sulfuric acid in new particle formation and growth
750 in the mega-city of Beijing, Atmos. Chem. Phys., 10, 4953-4960,
751 10.5194/acp-10-4953-2010, 2010.
752 Zhang, Q., Worsnop, D. R., Canagaratna, M. R., and Jimenez, J. L.: Hydrocarbon-like and
753 oxygenated organic aerosols in Pittsburgh: Insights into sources and processes of organic
754 aerosols, Atmos. Chem. Phys., 5, 3289-3311, 2005.
755 Zhang, Q., Jimenez, J. L., Canagaratna, M. R., Allan, J. D., Coe, H., Ulbrich, I., Alfarra, M. R.,
756 Takami, A., Middlebrook, A. M., Sun, Y. L., Dzepina, K., Dunlea, E., Docherty, K., DeCarlo, P.
757 F., Salcedo, D., Onasch, T., Jayne, J. T., Miyoshi, T., Shimono, A., Hatakeyama, S., Takegawa,
758 N., Kondo, Y., Schneider, J., Drewnick, F., Borrmann, S., Weimer, S., Demerjian, K.,
759 Williams, P., Bower, K., Bahreini, R., Cottrell, L., Griffin, R. J., Rautiainen, J., Sun, J. Y.,
760 Zhang, Y. M., and Worsnop, D. R.: Ubiquity and dominance of oxygenated species in
761 organic aerosols in anthropogenically-influenced Northern Hemisphere midlatitudes,
762 Geophys. Res. Lett., 34, L13801,10.1029/2007gl029979, 2007a.
763 Zhang, Q., Jimenez, J. L., Worsnop, D. R., and Canagaratna, M.: A case study of urban particle
764 acidity and its effect on secondary organic aerosol, Environ. Sci. Technol., 41, 3213-3219,
765 2007b.
766 Zhang, Q., Jimenez, J. L., Canagaratna, M. R., Ulbrich, I. M., Ng, N. L., Worsnop, D. R., and Sun,
767 Y.: Understanding atmospheric organic aerosols via factor analysis of aerosol mass
768 spectrometry: a review, Anal. Bioanal. Chem., 401, 3045-3067,
769 10.1007/s00216-011-5355-y, 2011a.
770 Zhang, Y. J., Tang, L. L., Wang, Z., Yu, H. X., Sun, Y. L., Liu, D., Qin, W., Canonaco, F., Prévôt, A. S.
771 H., Zhang, H. L., and Zhou, H. C.: Insights into characteristics, sources, and evolution of
772 submicron aerosols during harvest seasons in the Yangtze River delta region, China,
773 Atmos. Chem. Phys., 15, 1331-1349, 10.5194/acp-15-1331-2015, 2015.
774 Zhang, Y. M., Zhang, X. Y., Sun, J. Y., Lin, W. L., Gong, S. L., Shen, X. J., and Yang, S.:
775 Characterization of new particle and secondary aerosol formation during summertime in
776 Beijing, China, Tellus B, 63, 382-394, 10.1111/j.1600-0889.2011.00533.x, 2011b.
777 Zhang, Y. M., Zhang, X. Y., Sun, J. Y., Hu, G. Y., Shen, X. J., Wang, Y. Q., Wang, T. T., Wang, D. Z.,
778 and Zhao, Y.: Chemical composition and mass size distribution of PM₁ at an
779 elevated site in central east China, Atmos. Chem. Phys., 14, 12237-12249,
780 10.5194/acp-14-12237-2014, 2014.
781 Zhao, Z. Z., Cao, J. J., Shen, Z. X., Xu, B. Q., Zhu, C. S., Chen, L. W. A., Su, X. L., Liu, S. X., Han, Y.
782 M., Wang, G. H., and Ho, K. F.: Aerosol particles at a high-altitude site on the Southeast

783 Tibetan Plateau, China: Implications for pollution transport from South Asia, J. Geophys.
784 Res.-Atmos., 118, 11360-11375, 10.1002/jgrd.50599, 2013.

Tables

Table 1. A summary of average mass concentrations (μg m^{-3}) of PM_1 species during five episodes and the entire study. The 30 min detection limit (DLs) of the ACSM is also shown (Sun et al., 2012).

	Org	SO_4	NO_3	NH_4	Cl	BC	PM_1
Entire Study	4.9	3.2	1.2	1.4	0.14	0.51	11.9
Clean1	1.2	1.3	0.25	0.58	0.02	0.22	3.6
Clean2	1.8	1.3	0.24	0.45	0.03	-	3.8
Ep1	19.1	2.1	2.7	1.4	0.53	1.4	27.2
Ep2	6.3	5.9	2.0	2.6	0.18	0.57	17.6
Ep3	10.8	6.0	2.9	2.6	0.39	1.0	23.7
DLs	0.54	0.07	0.06	0.25	0.03		

Figure Captions:

Figure 1. Map of the sampling site (Menyuan, Qinghai). Also shown is the chemical composition of submicron aerosols measured at selected rural/remote sites in East Asia except Lanzhou, an urban site in northwest China. The detailed information of the sampling sites is presented in Table S1.

Figure 2. Comparison of the mass concentrations of PM_1 (NR-PM_1 +BC) measured by the ACSM and Aethalometer with that by the SMPS (D_m = 12 – 478 nm): (a) time series and (b) scatter plot.

Figure 3. Time series of (a-c) meteorological variables including T (temperature), RH (relative humidity), Precip. (precipitation), WS (wind speed), WD (wind direction), and Vis (visibility), (d) mass concentrations and (e) mass fractions of PM_1 species . The pie charts show the average chemical composition of PM_1 for five episodes.

Figure 4. Average diurnal cycles of (a) mass concentration; (b) mass fraction of PM_1 species; (c) ratios of aerosol species to CO, and (d) gaseous species. The local sunrise and sunset was around 7:00 and 19:00, respectively.

Figure 5. (a) Mass spectra and (b) time series of mass concentrations of BBOA and OOA. The standard average mass spectra of BBOA and OOA in Ng et al. (2011)are also shown for the comparison. The pie chart in (b) shows the average composition of OA for the entire study.

Figure 6. Scatter plot of OOA versus SO_4 during BB and NBB periods. The data points are color coded by BBOA concentrations. The pie chart shows the average composition of OA with post-processed OOA (= OOA – SO_4× $[OOA/SO_4]_{NBB}$).

Figure 7. (a) The evolution of particle number size distributions; (b) average particle number size distributions during NPE and non-NPE; (c,d) time series and diurnal cycles of particle number concentrations for three different sizes. The log-normal distribution fitting of each mode is shown in (b) as dash lines. The sunrise time was around 7:00.

Figure 8. Diurnal evolution of particle size distributions, aerosol composition, gaseous precursors, and the ratios of aerosol species to CO during (a) NPE and (b) non-NPE. The sunrise time was approximately 7:00.

Figure 9. (a) Time series of OOA/PM_1, particle growth rates, and average chemical composition during particle growth periods; (b) correlation of growth rate with OOA/PM_1. The data points are color coded by the PM_1 mass concentration.

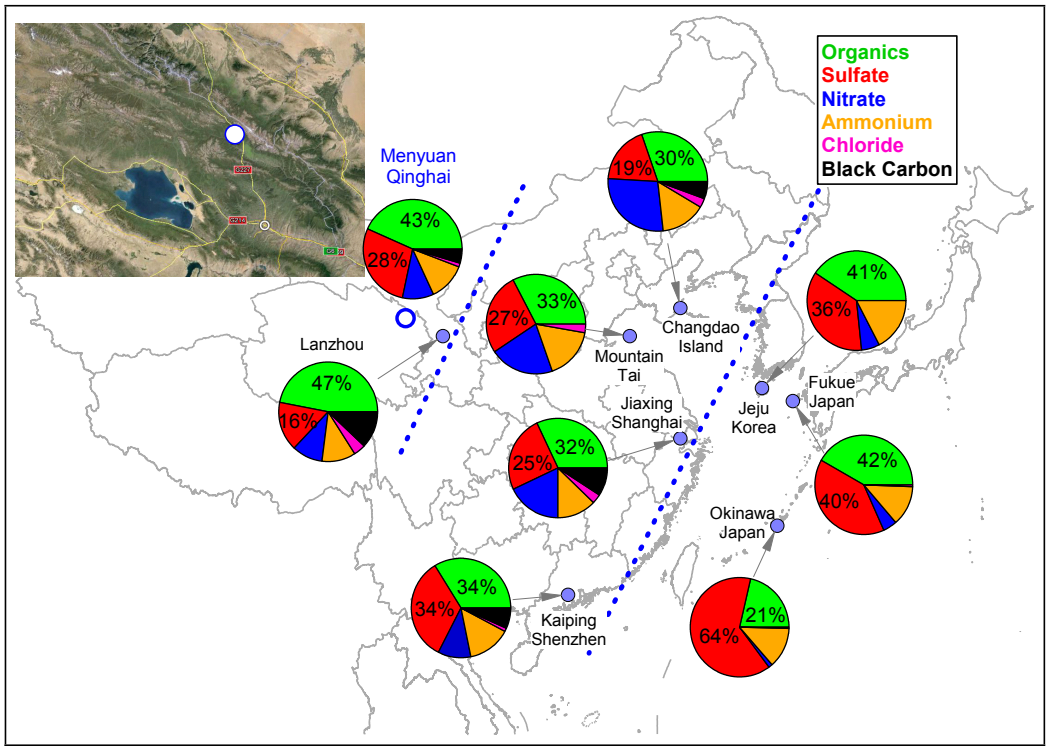

825

826 Figure 1. Map of the sampling site (Menyuan, Qinghai). Also shown is the chemical
827 composition of submicron aerosols measured at selected rural/remote sites in East
828 Asia except Lanzhou, an urban site in northwest China. The detailed information of
829 the sampling sites is presented in Table S1.

830

831

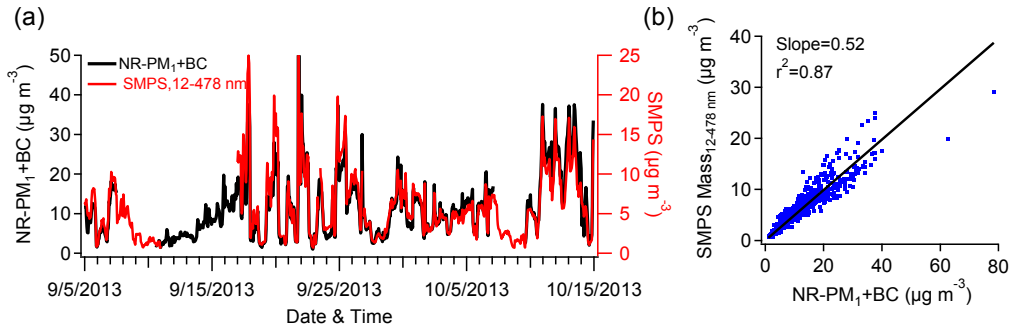

832

833 Figure 2. Comparison of the mass concentrations of PM_1 (NR-PM_1 +BC) measured
834 by the ACSM and Aethalometer with that by the SMPS (D_m = 12 – 478 nm): (a) time
835 series and (b) scatter plot.

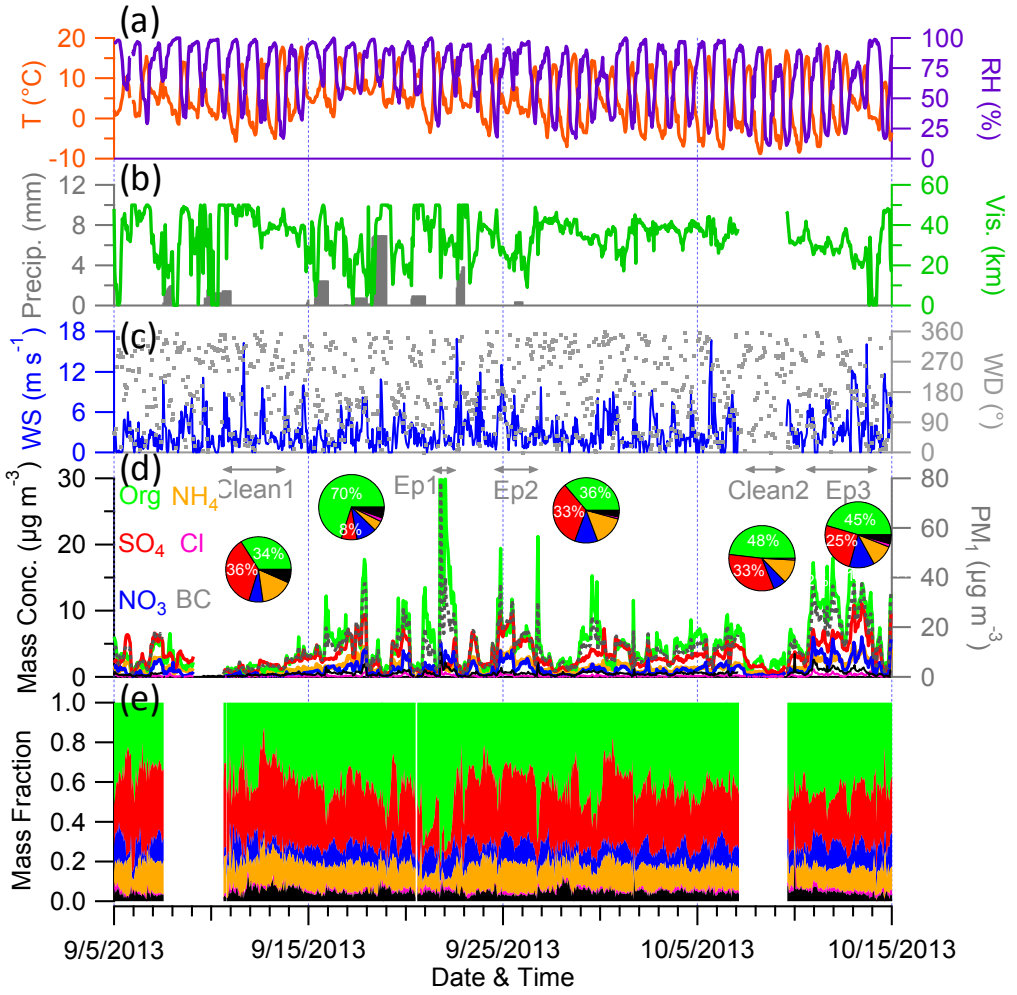

Figure 3. Time series of (a-c) meteorological variables including T (temperature), RH (relative humidity), Precip. (precipitation), WS (wind speed), WD (wind direction), and Vis (visibility), (d) mass concentrations and (e) mass fractions of PM_1 species . The pie charts show the average chemical composition of PM_1 for five episodes.

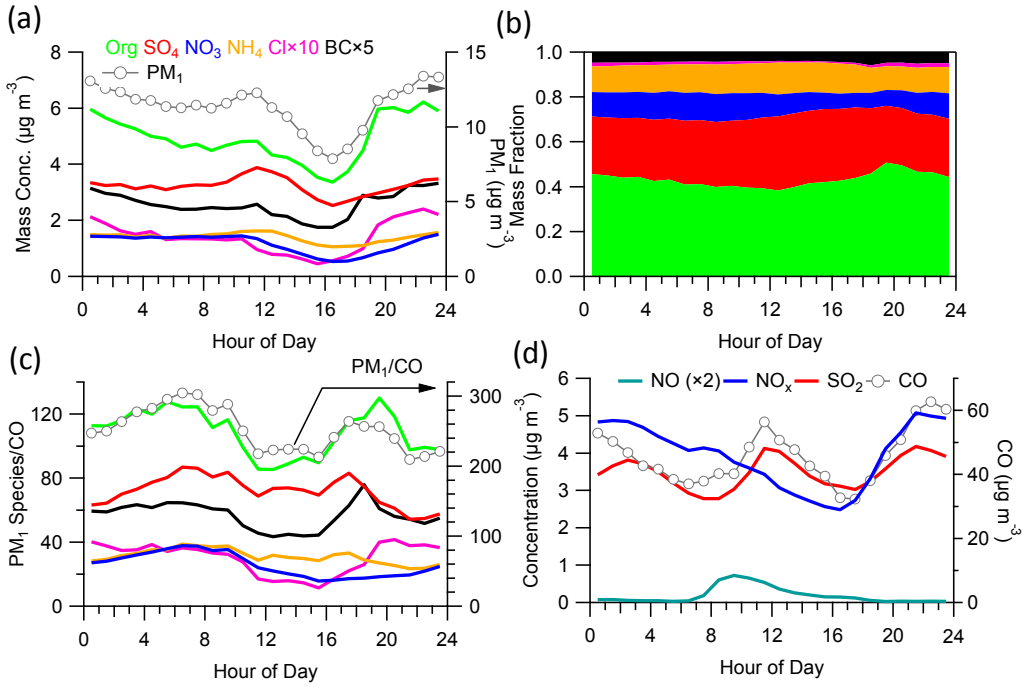

841

842 Figure 4. Average diurnal cycles of (a) mass concentration; (b) mass fraction of PM_1
843 species; (c) ratios of aerosol species to CO, and (d) gaseous species. The local sunrise
844 and sunset was around 7:00 and 19:00, respectively.

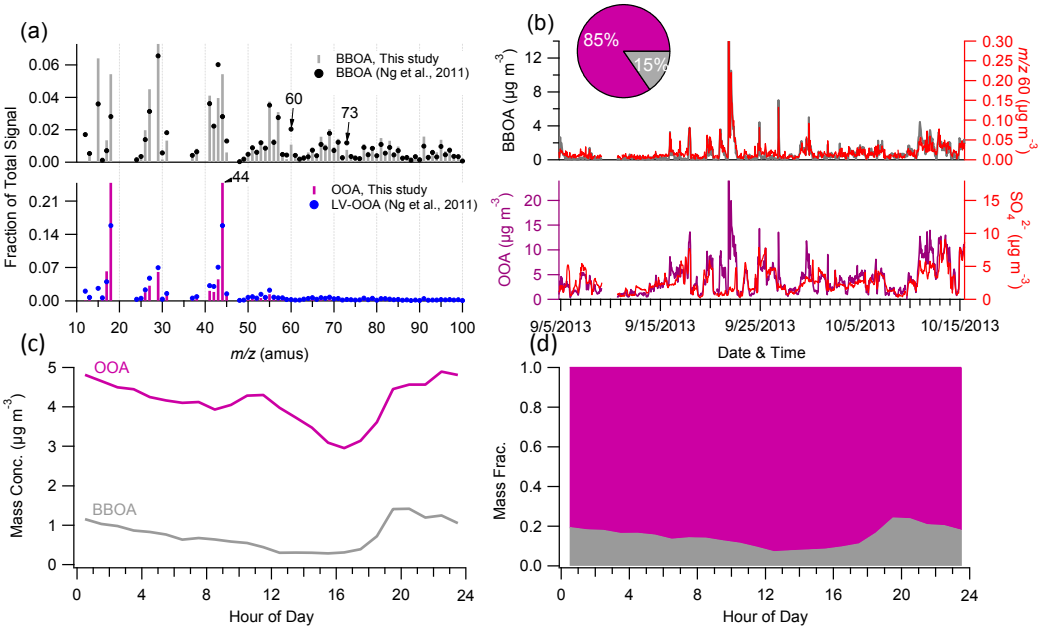

845

846 Figure 5. (a) Mass spectra and (b) time series of mass concentrations of BBOA and
847 OOA, (c) and (d) show the average diurnal cycles of BBOA and OOA. In addition,
848 the standard average mass spectra of BBOA and OOA in Ng et al. (2011) are also
849 shown in (a) for the comparison. The pie chart in (b) shows the average composition
850 of OA for the entire study.

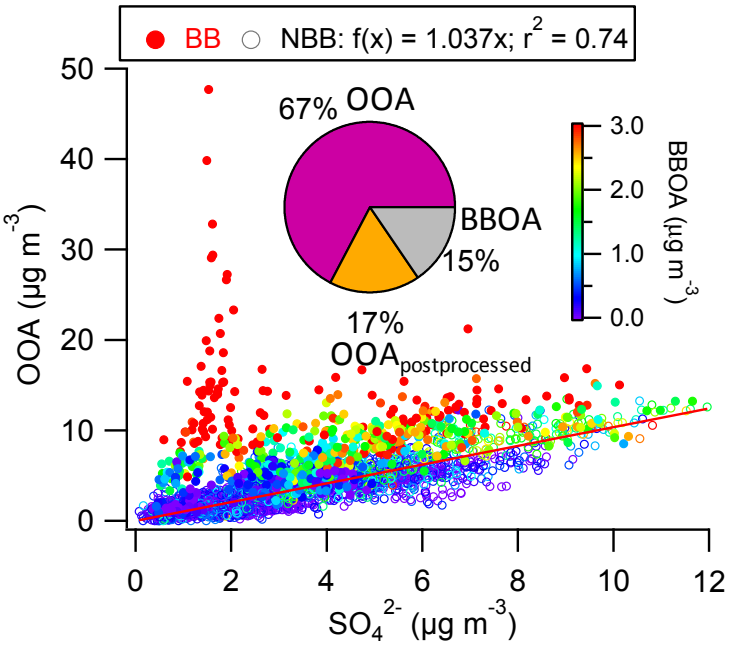

Figure 6. Scatter plot of OOA versus SO_4 during BB and NBB periods. The data points are color coded by BBOA concentrations. The pie chart shows the average composition of OA with post-processed OOA (= OOA – SO_4× $[OOA/SO_4]_{NBB}$).

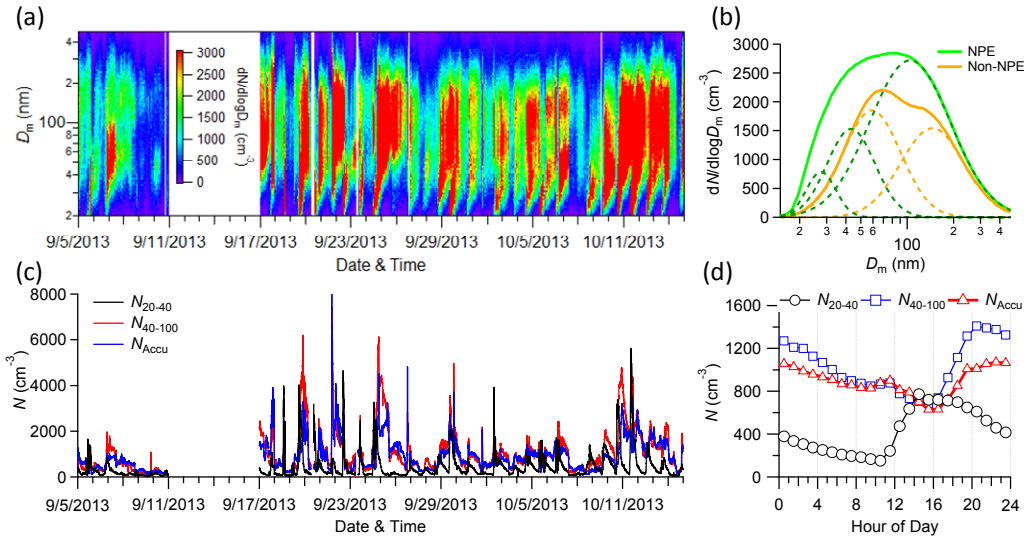

Figure 7. (a) The evolution of particle number size distributions; (b) average particle number size distributions during NPE and non-NPE; (c,d) time series and diurnal cycles of particle number concentrations for three different sizes. The log-normal distribution fitting of each mode is shown in (b) as dash lines. The sunrise time was around 7:00.

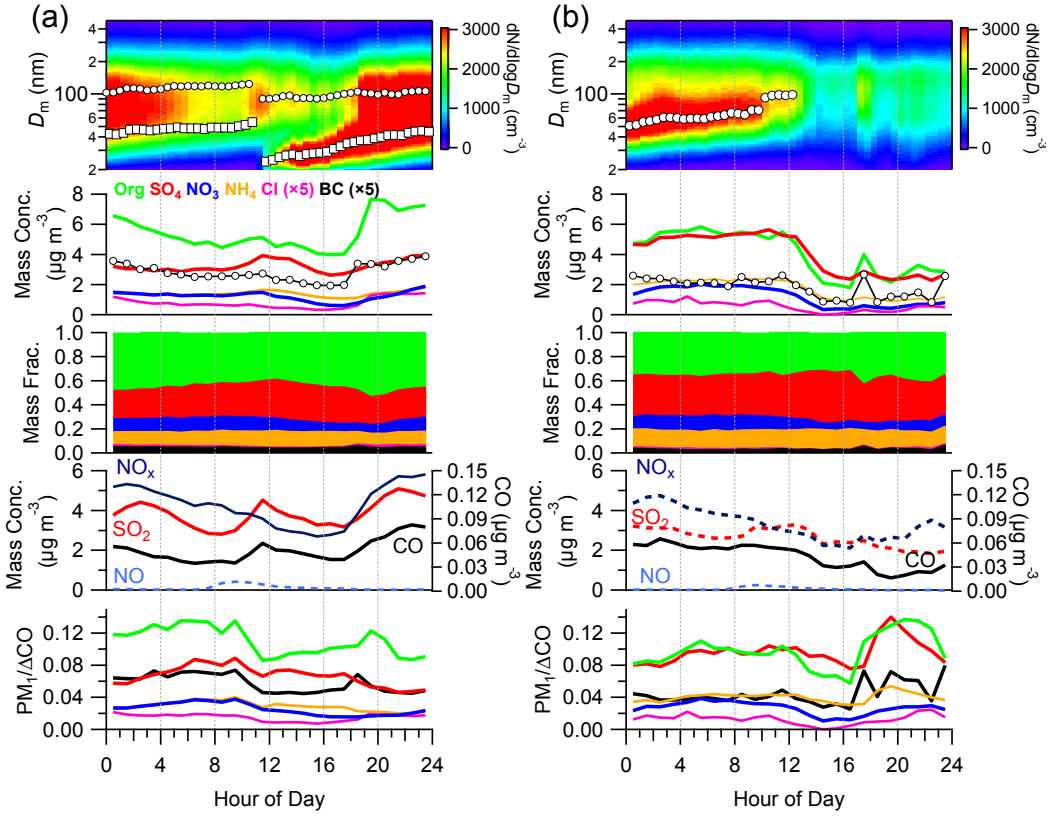

Figure 8. Diurnal evolution of particle size distributions, aerosol composition, gaseous precursors, and the ratios of aerosol species to CO during (a) NPE and (b) non-NPE. The sunrise time was approximately 7:00.

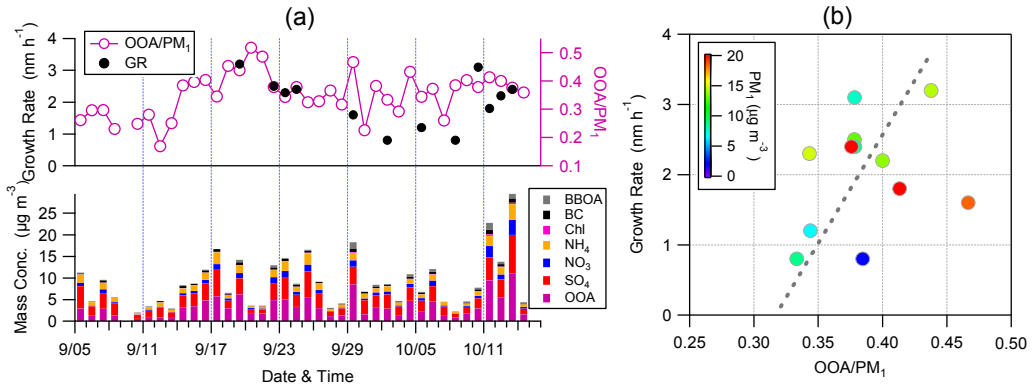

Figure 9. (a) Time series of OOA/PM_1, particle growth rates, and average chemical composition during particle growth periods; (b) correlation of growth rate with OOA/PM_1. The data points are color coded by the PM_1 mass concentration.